Nano Energy 31 (2017) 568–574

Contents lists available at ScienceDirect

Nano Energy

journal homepage: www.elsevier.com/locate/nanoen

Conductive graphene oxide-polyacrylic acid (GOPAA) binder for lithium-sulfur battery

Guiyin Xu[a,b], Qing-bo Yan[b,c], Akihiro Kushima[b], Xiaogang Zhang[a,*], Jin Pan[a], Ju Li[b,*]

[a] Jiangsu Key Laboratory of Material and Technology for Energy Conversion, College of Material Science and Engineering, Nanjing University of Aeronautics and Astronautics, Nanjing 210016, China

[b] Department of Nuclear Science and Engineering and Department of Materials Science and Engineering, Massachusetts Institute of Technology, Cambridge, MA 02139, USA

[c] College of Materials Science and Opto-Electronic Technology, University of Chinese Academy of Sciences, Beijing 100049, China

ARTICLE INFO

Keywords:
Polysulfides adsorption
Electrocatalysis
Peel test
Electrochemical impedance spectroscopy

ABSTRACT

Lithium-sulfur batteries have high cathode theoretical energy density, but the poor conductivity of sulfur and polysulfide shuttling result in serious polarization and low sulfur utilization. Moreover, the addition of insulating binder in the electrode increases the internal resistance, reducing specific capacity and rate performance. Herein, we develop a composite binder with higher electronic conductivity, superior mechanical property and strong adsorption of polysulfides that imparts it some electrocatalytic activity. The reduced graphene oxide- polyacrylic acid (GOPAA) binder is prepared *via* a simple solution process. At constant loading fraction of 10 wt%, using GOPAA binder induces a 30% enhancement in the cathode capacity, better cycle life and rate capability compared to using PAA binder, reducing both the local charge-transfer resistance and the global electronic resistance before and after cycling. These are attributed to the enhanced binding strength and synergistic effect of reduced graphene oxide and PAA forming well-dispersed conductive bridges to promote rapid electron transfer. Additionally, GOPAA provides active sites for adsorption of lithium polysulfides and electrocatalytic activity, shifting redox peaks in cyclic voltammetry and improving roundtrip efficiency.

1. Introduction

Developing high-performance energy storage systems is of great importance for society and environment [1,2]. Among the various types of rechargeable batteries, lithium-sulfur (Li-S) batteries have attracted much attention due to their high cathode theoretical energy density (2600 Wh kg^{-1}), which is 3–5× that of commercialized cathodes, such as $LiMn_2O_4$, $LiCoO_2$, and $LiFePO_4$[3,4]. However, there are two major problems that hinder the practical application of Li-S batteries: (1) The poor electronic conductivity of sulfur and its solid discharge products (Li_2S/Li_2S_2) leads to the low utilization of sulfur and reduces the practical cathode specific capacity to less than the theoretical capacity of 1675 mAh g^{-1}[5,6,7]. (2) Soluble lithium polysulfide intermediates formed during the charge-discharge process can easily diffuse in the liquid electrolyte and cross over to the lithium anode, which causes rapid capacity fading [8–10]. Many efforts have been made to improve the electrochemical performance of Li-S batteries [11]. Commonly employed approach is to incorporate sulfur into nano-sized hosts such as carbon [12,13], polymer [14,15], and metal oxide [16] to form composite like KJC/S, a composite of sulfur and Ketjenblack carbon (KJC).

In electrodes, binder holds the active material and electron conductive agents together and intimately bonds them to the current collector [17]. Even though binder takes up only a small fraction of the dried electrode weight (usually 10 wt%), it plays a disproportionally important role, being the bridge that has to maintain connections. Conventional binders are usually electronically insulating polymers such as polyacrylic acid (PAA) [18], polyvinylidene fluoride (PVDF) [19], polyoxyethylene oxide (PEO) [20] and LA132 [21], which increase the internal resistance of the electrodes. So naturally there is desire to develop a new kind of binder with high electrical conductivity. Conductive polymers have been used as binders to prepare sulfur cathodes. Liu et al.[22] reported the conductive polymer poly(3,4-ethylenedioxythiophene) (PEDOT) as a conductive binder for Li-S batteries and demonstrated a increase in the electrochemical performance of sulfur cathodes. But it has been pointed out that most conducting polymers have unsatisfactory mechanical properties (adhesion strength), and limited conductivity [23,24], thus the balance between bonding strength and conductivity needs to be explored.

In addition to improving the obvious *global* electronic conductivity

* Corresponding authors.
E-mail addresses: azhangxg@nuaa.edu.cn (X. Zhang), liju@mit.edu (J. Li).

http://dx.doi.org/10.1016/j.nanoen.2016.12.002
Received 25 July 2016; Received in revised form 2 December 2016; Accepted 2 December 2016
Available online 05 December 2016

R_{global}, there is also another *local* electrocatalytic aspect of the binder that may need to be considered. Because binder bridges the sulfur-containing active material with electron donor, they are crucial for controlling the charge transfer resistance (R_{ct}), that characterizes the facileness of *local* redox reactions whereby the active material receives an electron (thus may have to cross the "bridge"–the binder), and simultaneously captures a solvated Li^+ from the liquid electrolyte, breaking its solvation shell and accomplishing redox of the sulfide in the process. These are molecular scale processes, so minute details of the binder surface (such as how well the liquid electrolyte wets it, and how well it adsorbs lithium sulfides) may matter. One can use electrochemical impedance spectroscopy (EIS) to measure R_{global} and R_{ct} of the electrode before and after cycling. Also, the electrocatalytic activity will show up in cyclic voltammetry (CV) tests.

Graphene has the advantages of high specific area, superior electrical conductivity, and mechanical flexibility [25,26]. It is feasible to combine the flexible and conductive graphene with the insulating polymer binder to obtain a bi-function binder. Oh et al.[27] applied a highly conductive graphene as a nanofiller for PVDF binder and directly used the nanocomposite as a conductive binder for lithium titanium oxide (LTO) electrodes. However, the cycling performance of Li-S batteries based on PVDF binder is poorer than that of PAA binder [18]. PAA, a type of glue-like binder, has strong adhesion strength and can better restrain the electrode material desquamation due to large volume change and stress evolution in conversion electrodes.

In this work, we develop a conductive binder which consists of reduced graphene oxide (RGO) and PAA, termed GOPAA. The amount of RGO in GOPAA is really small, only 1/10th of the GOPAA weight. As GOPAA occupies 10 wt% of the cathode, the total amount of RGO in the cathode is only 1 wt%. But huge improvements in performance and cycle life are seen compared to using PAA binder alone at 10 wt%, indicating the disproportional importance of the binder.

2. Experimental section

2.1. Synthesis of reduced graphene oxide, GOPAA binder and KJC/S composite

Graphene oxide (GO) was synthesized by a modified Hummers' method, which used natural flake graphite as the precursor [28]. Then, the obtained graphene oxide was reduced using the saturated vapor of dimethylhydrazine and further reduced by annealing in nitrogen for 5 h at 200 °C [29]. Finally, the material was cooled to room temperature and reduced graphene oxide (RGO) was obtained.

To prepare the GOPAA binder, 4 mg RGO was added into 3.2 mL N-methyl pyrrolidinone (NMP) and sonicated for 2 h to form a uniform dispersion. Then, 36 mg PAA was incorporated into the above solution with vigorous stirring under 70 °C for 24 h in a sealed system. The obtained composite conductive binder was named GOPAA.

To synthesize the KJC/S composite, sulfur and Ketjenblack carbon (KJC) were mixed at a mass ratio of 7:3. Then, the mixture was heated at 155 °C for 10 h in order to melt sulfur into the pores of the carbon matrix.

2.2. Materials characterization

Fourier transform infrared spectroscopy (FT-IR, Thermo Scientific, Nicolet 750) was recorded to analyze the interaction between PAA and RGO in GOPAA in spectral range of 4000–400 cm^{-1}. X-ray diffraction (XRD) was conducted using a Bruker-AXS D8 DISCOVER equipped with a Cutarget X-ray tube between 10° and 80°. Thermogravimetric (TG) analysis was measured on a TG-DSC instrument (NETZSCH STA 409 PC) at a heating rate of 10 °C min^{-1} from 25 to 500 °C in nitrogen. The surface morphology and dispersion of RGO on the electrodes were observed using a scanning electron microscope (SEM) (Hitachi S-4800, Japan). Transmission electron microscopy (TEM) (JEOL JEM-2010) and Scanning transmission electron microscopy (STEM) (Tecnai G2 F20) were used to characterize the dispersion of sulfur in active materials. The X-ray photoelectron spectroscopy (XPS) analysis was performed on a Perkin-Elmer PHI 550 spectrometer with Al Kα (1486.6 eV) as the X-ray source. The 180° peel strength of the dried electrode coating on aluminum current collector was tested on a Peel Tester HY-0230 with a roller press of 10 times, a force of 100 N, and a speed of 100 mm min^{-1} at 25 °C.

2.3. Electrochemical characterization

Electrochemical characterization was carried out in a CR2016-type coin cell. A slurry coating procedure was taken to prepare the sulfur electrodes. In particular, active materials, conductive agent (acetylene black) and binder (PAA or GOPAA) were mixed together to form slurries with N-methyl pyrrolidinone (NMP) as solvent. Then, the slurries were homogeneously coated onto aluminum foil current collectors. Finally, the electrodes were dried at 60 °C for 12 h in vacuum oven to evaporate NMP. The typical loading of sulfur was approximately 0.8 mg cm^{-2}. The test cells were fabricated in an argon-filled glove box using the sulfur electrode as working electrode, lithium metal foil as the counter electrode and porous polypropylene (PP) membrane as the separator. The electrolyte was the mixing of 1, 3-dioxolane (DOL) and 1, 2-dimethoxyethane (DME) (volume ratio 1:1) with 1 M LiTFSI and 0.1 M $LiNO_3$. The amount of the electrolyte used in the cells was ~20 μL. The galvanostatic discharge-charge tests were measured on a CT2001A cell test instrument (LAND Electronic Co.) between 1.7 and 3.0 V (*vs.* Li/Li^+). The cyclic voltammetry (CV) was conducted on a CHI660D electrochemical workstation (Shanghai Chenhua, China). Electrochemical impedance measurements (EIS) were conducted in the frequency range of 10^{-2}-10^5 Hz with the amplitude of 5 mV.

2.4. Computational modeling

Theoretical calculations of lithium sulfides adsorption were carried out by using Vienna ab initio simulation package (VASP) [30], which was based on density functional theory (DFT) [31] and the projected augmented wave (PAW) method [32]. Generalized gradient approximation (GGA) in the form of Perdew-Burke-Ernzerhof (PBE) [33] was chosen as exchange correlation potential. The kinetic energy cutoff was set to 500 eV. All structures were fully optimized and the maximum force on each atom was less than 0.01 eV $Å^{-1}$. Various initial adsorption configurations have been considered, and the most stable optimized configuration is presented in Fig. 1. The adsorption energy (E_a) is defined as the difference between the total energy (E_{tot}) of Li_2S (LiS*)-PAA compound, and the energy sum of Li_2S (LiS*) ($E_{Li_2S/LiS*}$) and PAA (E_{PAA}): $E_a = E_{Li_2S/LiS*} + E_{PAA} - E_{tot}$.

3. Results and discussion

PAA can chemically adsorb lithium polysulfides by the Li-O bond (Fig. 1a, c). The lengths of the Li-O bond formed with Li_2S and LiS* were calculated to be 1.84 and 1.93 Å, respectively. The coterminous oxygen in PAA also has an interaction with lithium polysulfides (the dotted line in Fig. 1a, c), thereby further increasing the adsorption strength. The adsorption energies of Li_2S and Li-S* on PAA were 1.44 and 1.31 eV, respectively. PAA has a higher binding energy with lithium polysulfides compared with PVDF (Table S1). Therefore, the cycling performance of Li-S batteries based on PAA is better than that based on PVDF [10,18]. To confirm the bond formation, the differential charge densities around Li_2S and LiS* were calculated from the difference of Li_2S (LiS*)-PPA compound charge density and the sum of Li_2S (LiS*) charge density and PPA charge density (Fig. 1b, d). The blue color represents the charge density decrease, while the green-yellow and orange colors correspond to charge density increase. The

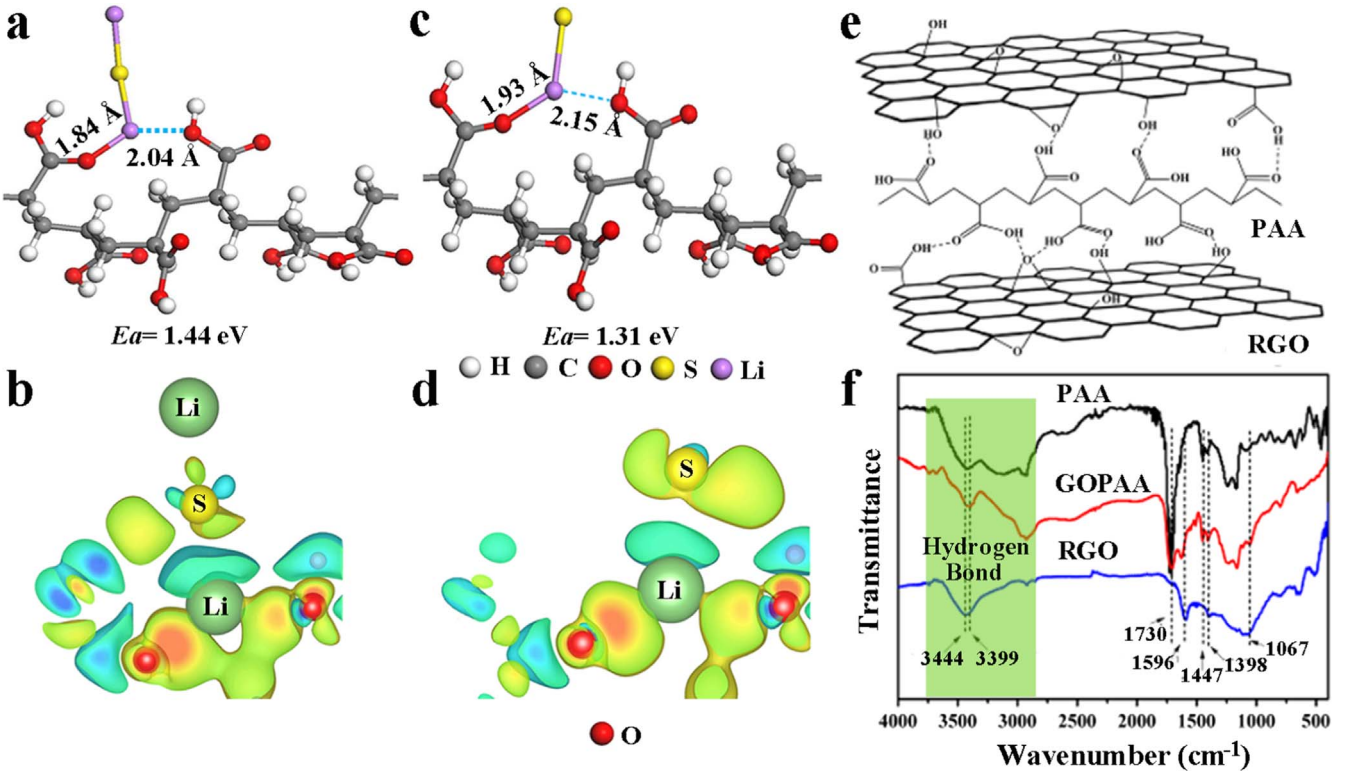

Fig. 1. Schematic structures of (a) Li_2S and (c) Li-S* adsorbed on PAA. The differential charge densities around (b) Li_2S and (d) LiS*. (e) Schematic illustration for the formation of hydrogen bonding between RGO and PAA. (f) Fourier transform infrared spectroscopy (FT-IR) spectra of PAA, RGO and GOPAA.

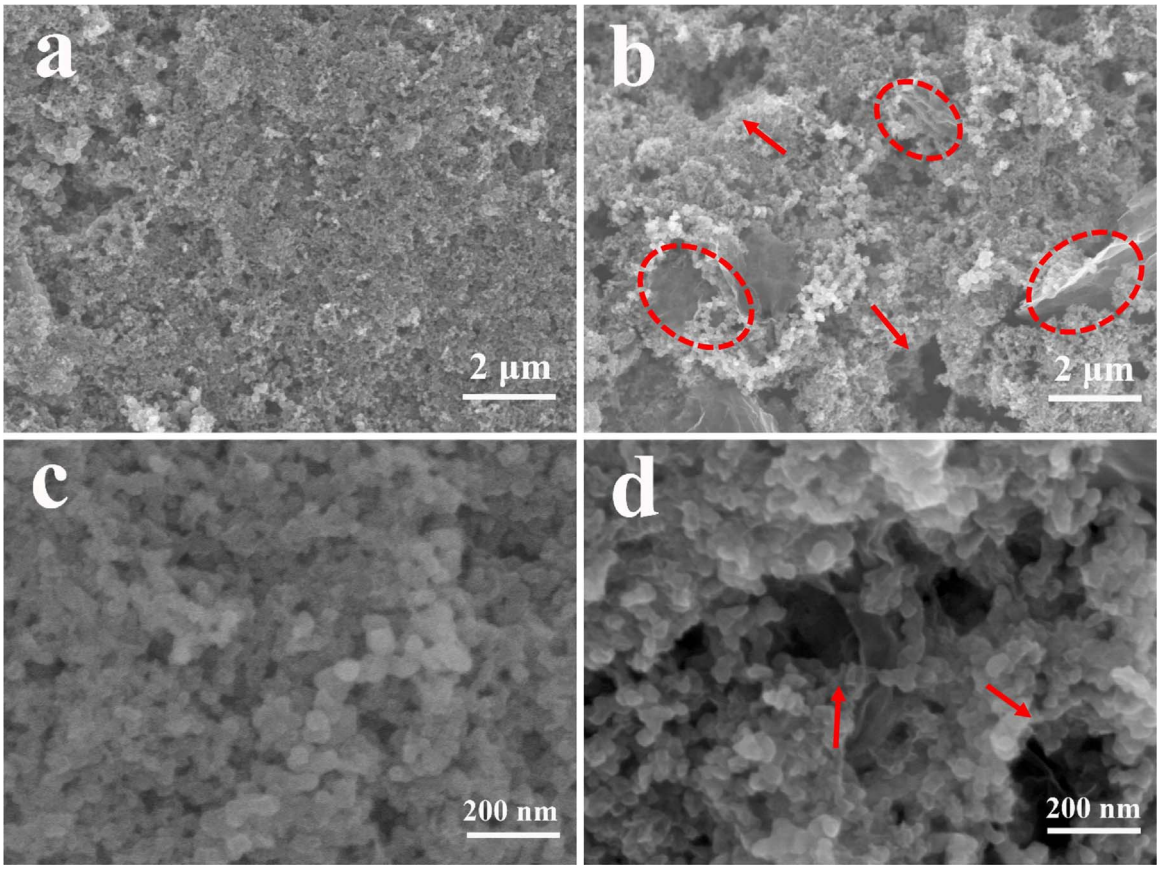

Fig. 2. Scanning electron microscope (SEM) images of (a, c) KJC/S PAA electrodes and (b, d) KJC/S GOPAA electrodes.

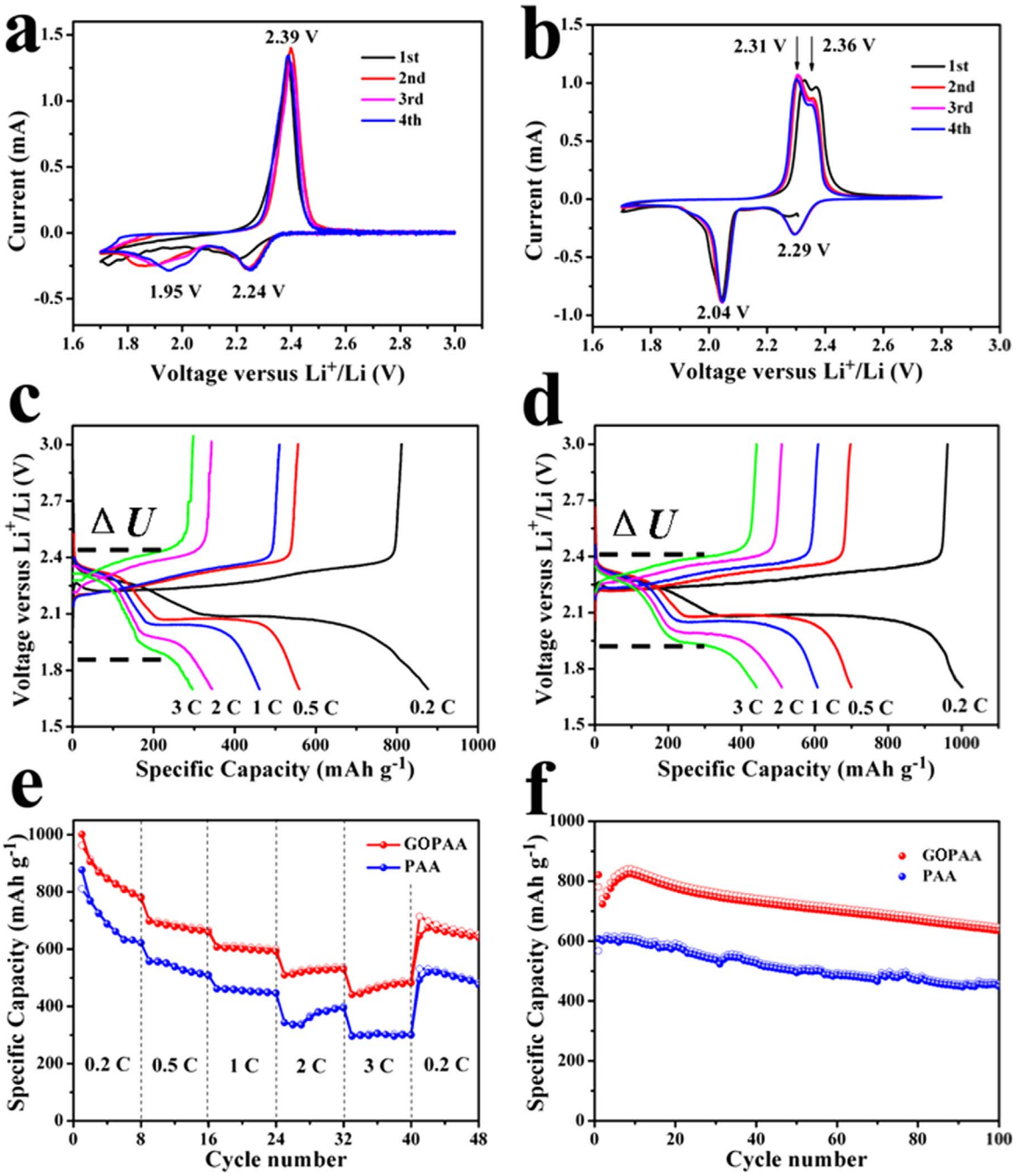

Fig. 3. Cyclic voltammetry (CV) of Li-S batteries with (a) PAA and (b) GOPAA binders at a scan rate of 0.1 mV s^{-1}. The charge-discharge profiles of Li-S batteries with (c) PAA and (d) GOPAA binders at various rates. (e) Rate capability and (f) cycling performance of Li-S batteries with different binders at 0.5 C.

result shows the decrease in the electron density between Li and S atoms and the increase between Li and O atoms, implying the Li atoms were strongly bound to O atoms.

GOPAA was prepared by a simple solution process of mixing PAA with RGO. The free carboxylic acid in PAA and the O-H, –COOH and C-O-C sites in RGO can form hydrogen bonds (Fig. 1**e)**. In the FT-IR spectrum of PAA (Fig. 1f), two absorption bands at 1730 and 1447 cm^{-1} correspond to the stretching vibrations of C=O and O-H from –COOH in PAA [34]. In the FT-IR spectrum of RGO, the bands at 3444, 1596 and 1067 cm^{-1} are attributed to the O-H, -COOH and C-O-C stretching vibrations, respectively [35,36]. In the FT-IR spectra of PAA and GOPAA, the bands from 3700 to 2800 cm^{-1} correspond to the hydrogen bond. The band around 3200–3500 cm^{-1} in GOPAA shifts to a lower wavenumber compared to PAA, which result from the dissociation of the hydrogen bonding among –COOH groups in PAA [37,38]. These results demonstrate that hydrogen bonding exists between PAA and RGO, which contributes to the homogeneous dispersion of RGO. The as-prepared RGO shows a laminar wrinkle structure (Fig. S2a) and there is no obvious morphology change in GOPAA (Fig. S2B), thus the high conductive property of RGO should be maintained. The uniformly distributed RGO not only act as electron transport channels but also provide large active sites for the reversible conversion between S_8/S_8^{2-} and Li_2S_2/Li_2S.

In fabricating the electrodes, the weight ratio of KJC/S, acetylene black and binder was 85: 5: 10, with nearly 60 wt% sulfur in the electrode (Fig. S3b). The average adhesion strength of PAA and GOPAA electrode measured from peel test is 111.36 and 158.55 mN mm^{-1}, respectively. The enhancement in peel strength of GOPAA electrode

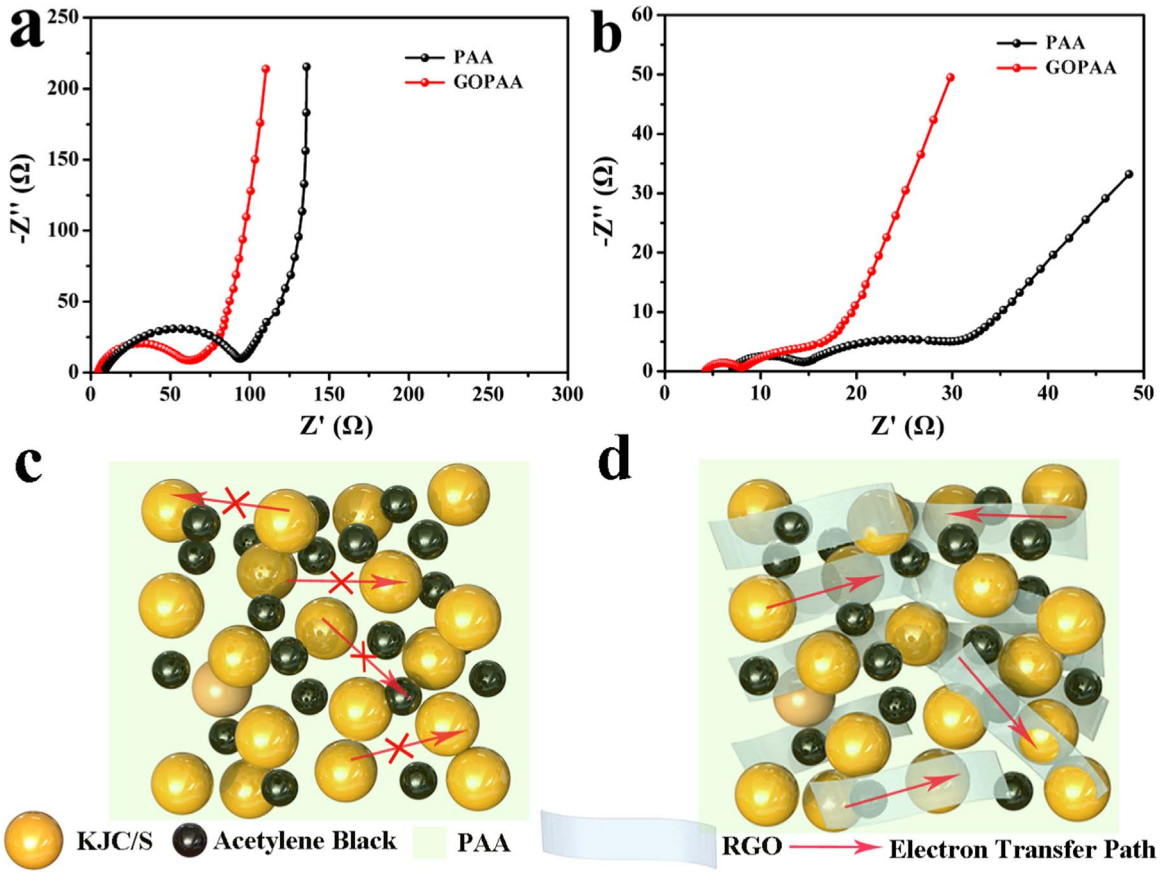

Fig. 4. Electrochemical impedance spectroscopy (EIS) tests of PAA and GOPAA electrodes (a) before cycling and (b) after 100 cycles. Schematic diagram for the sulfur electrodes with (c) PAA and (d) GOPAA binders.

results from the better-dispersed binder in the cathode, despite the slightly lower mass loading of PAA (9 wt% in GOPAA electrode *vs* 10 wt% in PAA electrode). The morphology of KJC/S electrodes with different binders is shown in Fig. 2. The KJC/S PAA electrodes clearly exhibit a compact structure with the aggregation of small particles (Fig. 2a, c). The KJC/S GOPAA electrodes, in contrast, show abundant pores with RGO nanosheets (red circle in Fig. 2b), favorable for liquid electrolyte infiltration and rapid ion diffusion. Many pores with diameter of ~200 nm are distributed on the surface of the GOPAA electrodes (red arrow in Fig. 2d) and the RGO nanosheets act as bridges penetrating the active materials, facilitating electron transport and electrocatalysis.

The typical CV curves of GOPAA and PAA electrodes at a scan rate of 0.1 mV s^{-1} are shown in Fig. 3a and b, respectively. For the PAA electrode, only one reduction peak can be observed at 2.21 V in the first cycle, indicating a serious polarization. After the first cycle, two reduction peaks appear at 2.24 and 1.95 V, corresponding to the transformation of elemental sulfur (S_8) to soluble lithium polysulfides (Li_2S_n, $4 \le n \le 8$), and then to insoluble Li_2S_2/Li_2S, respectively. The oxidation peak at ~2.39 V corresponds to the conversion of Li_2S_2/Li_2S to the long-chain lithium polysulfide (Li_2S_8) [39]. The GOPAA electrode exhibits two reduction peaks at ~2.29 and 2.04 V and two oxidation peaks at ~2.36 and 2.31 V, which shows significantly better roundtrip efficiency than PAA electrode. Importantly, the position and shape of these peaks obtained from different cycles (including the first cycle) are almost identical, demonstrating that the introduction of GOPAA conductive binder has electrocatalytic effects and improves the electrochemical reversibility.

The charge-discharge profiles of PAA and GOPAA electrodes at various rates are shown in Fig. 3c and d. The GOPAA electrodes still maintained the ~2.0 V lower discharge plateau at high rates, such as 2 C. Moreover, the voltage difference ΔU between charge and discharge plateaus of GOPAA electrodes was significantly smaller than that of PAA electrodes at the increased rates, indicating lower polarization and better roundtrip energy efficiency. At a current density of 0.2 C (1 C≡1675 mA g^{-1}), the discharge specific capacity of GOPAA electrodes reached 1000 mAh g^{-1} (Fig. 3e, specific capacities are calculated based on the mass of sulfur). Even at a high current density of 3 C, the GOPAA electrode showed a specific capacity of 464 mAh g^{-1}, demonstrating excellent rate performance. The GOPAA electrodes exhibited a 30% higher specific capacity than PAA electrodes at 0.5 C (Fig. 3f). The initial specific capacity of GOPAA electrode was ~820 mAh g^{-1}. Note the capacity gradually increased from the second to the fifth cycle, which can be attributed to the more porous structure of the GOPAA electrode that requires the activation steps to increase the utilization of active materials. After 100 cycles, the specific capacity of GOPAA electrode still remained at 635 mAh g^{-1}. For PAA electrode, the initial discharge specific capacity was about 607 mAh g^{-1} and decreased to 448 mAh g^{-1} after 100 cycles. The capacity decay rate of GOPAA (0.22%/cycle) was lower than that of PPA (0.26%/cycle).

To further clarify the mechanisms of improved battery performance, EIS tests of the PAA and GOPAA electrodes were conducted before and after 100 cycles. The EIS spectra of the PAA and GOPAA electrodes at fresh state are compared in Fig. 4a. The Nyquist plots of the two electrodes consist of a depressed semicircle at high frequency region and an oblique line at medium frequency region. The diameter of the depressed semicircle represents the charge transfer resistance (R_{ct}). The GOPAA electrode shows a much lower R_{ct} than that of the PAA electrode. R_{ct} characterizes the local redox reactions whereby the sulfur-containing active material receives an electron from conductive agents (RGO and carbon black), and simultaneously captures a lithium ion from the liquid electrolyte, breaking its solvation shell and

accomplish redox of the sulfides in the process. R_{ct} is different conceptually from R_{global}, the global (long-ranged) percolative transport of electrons, but R_{global} is also better in the GOPAA electrode as indicated by the smaller intercept at frequency→∞. For the cathodes after 100 cycles, the Nyquist plots exhibit two depressed semicircles and a sloping line (Fig. 4b). The GOPAA electrode not only exhibits much lower R_{ct} (*local*), but also much lower R_{global} compared with the PAA electrode after cycling. This may be ascribed to the following reasons: (a) GOPAA is a better binder mechanically, as indicated by the stronger adhesion in peel test, bringing the active material closer to the conductive agents. RGO is also an active substrate for the reversible deposition of Li_2S_2/Li_2S, thus reducing the distance and the activation barrier of the local redox reactions. (b) During cycling, there is large volume change in the sulfur-containing active solid, which can induce self-stress and disrupt the global electron transport network. But due to its better mechanical properties, the GOPAA binder provides a more effective electronic conductive network and a more stable interface structure than using PAA. The characteristics of two different binder electrodes for Li-S batteries are schematically shown in Fig. 4c and d. Compared with the PAA electrodes, the GOPAA electrodes increase the effective electrical contact area between the electrode materials, the current collector and the liquid electrolyte, as well as facilitating a stable long-range conductive network.

4. Conclusion

In summary, even though the binder takes up only a small fraction of the dried electrode weight (usually 10 wt%), it can play a disproportionally important role in battery performance, being the bridge that has to maintain connections between the active content, the electron source and ideally access to the liquid electrolyte. Because of its bridging role, it is also in an ideal position to mediate electrocatalysis involving multiple intermediate states of the lithium sulfides if it is conductive. So minute details of the binder surface (such as how well the liquid electrolyte wets it, and how well it adsorbs lithium sulfides) may matter. A novel conductive binder GOPAA was successfully prepared for sulfur cathodes, where we demonstrated ample hydrogen bonding between RGO and PAA, excellent dispersion, and maintenance of the conductivity and area of RGO. The GOPAA sulfur electrodes showed higher initial specific capacity, better rate performance, lower capacity decay rate and more favorable electrocatalytic kinetics. Inspired by these results, it might also be possible to disperse RGO by other chemical interactions, such as *in-situ* polymerization and covalent grafting, to obtain a multifunctional binder that gives high conductivity, superior peel strength, and low charge transfer resistance electrodes for lithium-ion batteries, sodium-ion batteries, lithium-air batteries, and lithium-sulfur batteries.

Acknowledgements

This work is supported by National Key Basic Research Program 973 (No. 2014CB239701), National Natural Science Foundation of China (No. 51372116), Natural Science Foundation of Jiangsu Province (No. BK2011030, BK20151468) and Fundamental Research Funds for the Central Universities of NUAA (NJ20160104). G.Y. Xu would like to thank Funding of Jiangsu Innovation Program for Graduate Education (KYLX15_0300), Outstanding Doctoral Dissertation in NUAA (BCXJ15-07) and China Scholarship Council (CSC). A. Kushima and J. Li acknowledge the support by NSF ECCS-1610806.

Appendix A. Supplementary material

Supplementary data associated with this article can be found in the online version at http://dx.doi.org/10.1016/j.nanoen.2016.12.002.

References

[1] N.S. Choi, Z. Chen, S.A. Freunberger, X. Ji, Y.K. Sun, K. Amine, G. Yushin, L.F. Nazar, J. Cho, P.G. Bruce, Angew. Chem. Int. Ed. 51 (2012) 9994–10024.
[2] P.G. Bruce, S.A. Freunberger, L.J. Hardwick, J.M. Tarascon, Nat. Mater. 11 (2012) 19–29.
[3] Y. Yang, G. Zheng, Y. Cui, Chem. Soc. Rev. 42 (2013) 3018–3032.
[4] X. Ji, K.T. Lee, L.F. Nazar, Nat. Mater. 8 (2009) 500–506.
[5] J.Q. Huang, X.F. Liu, Q. Zhang, C.M. Chen, M.Q. Zhao, S.M. Zhang, W. Zhu, W.Z. Qian, F. Wei, Nano Energy 2 (2013) 314–321.
[6] H. Xu, Y. Deng, Z. Zhao, H. Xu, X. Qin, G. Chen, Chem. Commun. 50 (2014) 10468–10470.
[7] Z. Li, L. Yuan, Z. Yi, Y. Sun, Y. Liu, Y. Jiang, Y. Shen, Y. Xin, Z. Zhang, Y. Huang, Adv. Energy Mater. 4 (2014). http://dx.doi.org/10.1002/aenm.201301473.
[8] J.Q. Huang, Q. Zhang, H.-J. Peng, X.Y. Liu, W.Z. Qian, F. Wei, Energy Environ. Sci. 7 (2014) 347–353.
[9] L. Suo, Y.S. Hu, H. Li, M. Armand, L. Chen, Nat. Commun. 4 (2013) 1481.
[10] Z.W. Seh, Q. Zhang, W. Li, G. Zheng, H. Yao, Y. Cui, Chem. Sci. 4 (2013) 3673–3677.
[11] G. Xu, B. Ding, J. Pan, P. Nie, L. Shen, X. Zhang, J. Mater. Chem. A 2 (2014) 12662–12676.
[12] G. Xu, B. Ding, P. Nie, L. Shen, J. Wang, X. Zhang, Chem. Eur. J. 19 (2013) 12306–12312.
[13] G. Xu, B. Ding, P. Nie, L. Shen, H. Dou, X. Zhang, A.C.S. Appl, Mater. Interfaces 6 (2014) 194–199.
[14] W. Li, Q. Zhang, G. Zheng, Z.W. Seh, H. Yao, Y. Cui, Nano Lett. 13 (2013) 5534–5540.
[15] G.C. Li, G.R. Li, S.H. Ye, X.P. Gao, Adv. Energy Mater. 2 (2012) 1238–1245.
[16] Z. Liang, G. Zheng, W. Li, Z.W. Seh, H. Yao, K. Yan, D. Kong, Y. Cui, ACS Nano 8 (2014) 5249–5256.
[17] S.L. Chou, Y. Pan, J.Z. Wang, H.K. Liu, S.X. Dou, Phys. Chem. Chem. Phys. 16 (2014) 20347–20359.
[18] Z. Zhang, W. Bao, H. Lu, M. Jia, K. Xie, Y. Lai, J. Li, ECS Electrochem. Lett. 1 (2012) A34–A37.
[19] J. Hassoun, B. Scrosati, Adv. Mater. 22 (2010) 5198–5201.
[20] M.J. Lacey, F. Jeschull, K. Edstrom, D. Brandell, Chem. Commun. 49 (2013) 8531–8533.
[21] J. Pan, G. Xu, B. Ding, J. Han, H. Dou, X. Zhang, RSC Adv. 5 (2015) 13709–13714.
[22] Z. Wang, Y. Chen, V. Battaglia, G. Liu, J. Mater. Res. 29 (2014) 1027–1033.
[23] G. Liu, S. Xun, N. Vukmirovic, X. Song, P. Olalde-Velasco, H. Zheng, V.S. Battaglia, L. Wang, W. Yang, Adv. Mater. 23 (2011) 4679–4683.
[24] P.R. Das, L. Komsiyska, O. Osters, G. Wittstock, J. Electrochem. Soc. 162 (2015) A674–A678.
[25] Z.S. Wu, G. Zhou, L.C. Yin, W. Ren, F. Li, H.M. Cheng, Nano Energy 1 (2012) 107–131.
[26] G. Zhou, L.C. Yin, D.W. Wang, L. Li, S. Pei, I.R. Gentle, F. Li, H.M. Cheng, ACS Nano 7 (2013) 5367–5375.
[27] S.W. Han, S.J. Kim, E.S. Oh, J. Electrochem. Soc. 161 (2014) A587–A592.
[28] M. Hirata, T. Gotou, S. Horiuchi, M. Fujiwara, M. Ohba, Carbon 42 (2004) 2929–2937.
[29] G. Eda, G. Fanchini, M. Chhowalla, Nat. Nano. 3 (2008) 270–274.
[30] G. Kresse, J. Furthmüller, Phys. Rev. B 54 (1996) 11169–11186.
[31] P. Hohenberg, W. Kohn, Phys. Rev. 136 (1964) B864–B871.
[32] G. Kresse, D. Joubert, Phys. Rev. B 59 (1999) 1758–1775.
[33] J.P. Perdew, K. Burke, M. Ernzerhof, Phys. Rev. Lett. 77 (1996) 3865–3868.
[34] L. Wang, D. Wang, F. Zhang, J. Jin, Nano Lett. 13 (2013) 4206–4211.
[35] S. Gao, H. Fan, Y. Chen, L. Li, Y. Bando, D. Golberg, Nano Energy 2 (2013) 1261–1270.
[36] F. Yang, M. Zhao, B. Zheng, D. Xiao, L. Wu, Y. Guo, J. Mater. Chem. 22 (2012) 25471–25479.
[37] L. Lu, H. Sun, F. Peng, Z. Jiang, J. Membr. Sci. 281 (2006) 245–252.
[38] X. Yang, L. Li, S. Shang, X.M. Tao, Polymer 51 (2010) 3431–3435.
[39] X. Yang, L. Zhang, F. Zhang, Y. Huang, Y. Chen, ACS Nano. 8 (2014) 5208–5215.

Guiyin Xu received his M.E. degrees in Applied Chemistry from Nanjing University of Aeronautics and Astronautics in 2014. He is currently pursuing his Ph.D. degree under the co-supervision of Prof. Xiaogang Zhang and Prof. Ju Li in the Department of Nuclear Science and Engineering at Massachusetts Institute of Technology. His research focuses on advanced electrode materials for energy storage devices, such as supercapacitors, lithium-ion batteries and Li-S batteries.

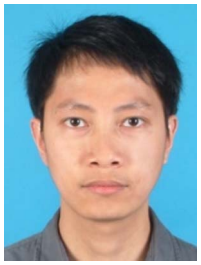

Qing-Bo Yan is an associate professor of University of Chinese Academy of Sciences (UCAS) and recently a visiting scholar in the Department of Nuclear Science and Engineering at Massachusetts Institute of Technology. His research interest is mainly on the physical properties of two-dimensional materials and energy storage materials through density functional theory based first-principles calculations and other atomistic simulation methods. Dr. Yan obtained his Ph.D. degree in the College of Physical Sciences at UCAS in 2009.

Akihiro Kushima is a Research Scientist in the Department of Nuclear Science and Engineering at Massachusetts Institute of Technology. His research interest is to understand the fundamental materials properties through combination of *in situ* electron microscopy and atomistic simulations with particular emphasis on energy storage materials. Dr. Kushima completed his Ph.D. and undergraduate studies in the Department of Engineering Physics and Mechanics at Kyoto University, Japan in 2007. Prior to his current position, he conducted postdoctoral studies at MIT (2007–2010) and University of Pennsylvania (2010–2012).

Xiaogang Zhang received his Ph. D. degree in Chemistry from Lanzhou University in 2001. He is now a professor of chemistry at College of Material Science and Engineering, Nanjing University of Aeronautics and Astronautics. His current research interests include the design and development of nanostructured composites and their applications in energy conversion and storage.

Jin Pan received her B. E. degree in Applied Chemistry from Nanjing University of Aeronautics and Astronautics in 2013. Now she studies in College of Material Science and Engineering at Nanjing University of Aeronautics and Astronautics for a master's degree under the supervision of Prof. Xiaogang Zhang. Her main research direction is new electrolytes and binders used in Li-S batteries.

Ju Li is BEA Professor of Nuclear Science and Engineering and Professor of Materials Science and Engineering at MIT. His group (http://Li.mit.edu) performs computational and experimental research on mechanical properties of materials, and energy storage and conversion. Ju was a recipient of the 2005 Presidential Early Career Award for Scientists and Engineers, 2006 MRS Outstanding Young Investigator Award, and 2007 TR35 award from *Technology Review* magazine. Ju was elected Fellow of the American Physical Society in 2014.

Supporting Information

Conductive Graphene Oxide-Polyacrylic Acid (GOPAA) Binder for Lithium-Sulfur Battery

Guiyin Xu, [a, b] Qing-bo Yan, [b, c] Akihiro Kushima, [b] Xiaogang Zhang, [a, *] Jin Pan, [a] Ju Li [b, *]

[a]Jiangsu Key Laboratory of Material and Technology for Energy Conversion, College of Material Science and Engineering, Nanjing University of Aeronautics and Astronautics, Nanjing 210016, China

[b]Department of Nuclear Science and Engineering and Department of Materials Science and Engineering, Massachusetts Institute of Technology, Cambridge, Massachusetts 02139, USA

[c]College of Materials Science and Opto-Electronic Technology, University of Chinese Academy of Sciences, Beijing 100049, China

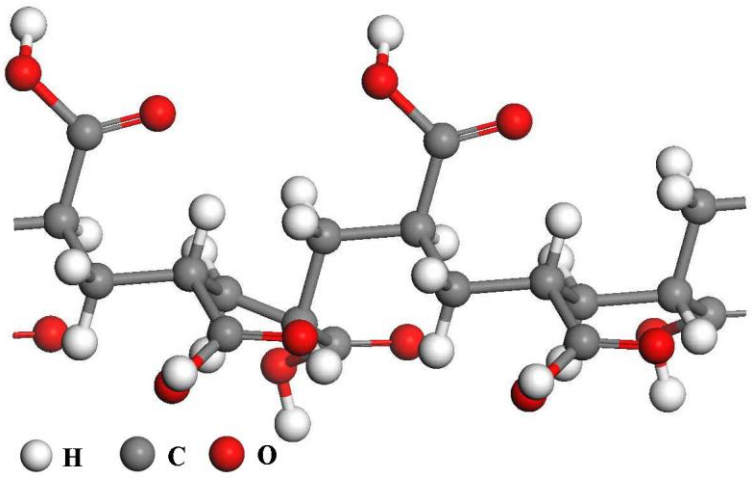

Figure S1. The optimized geometry of PAA.

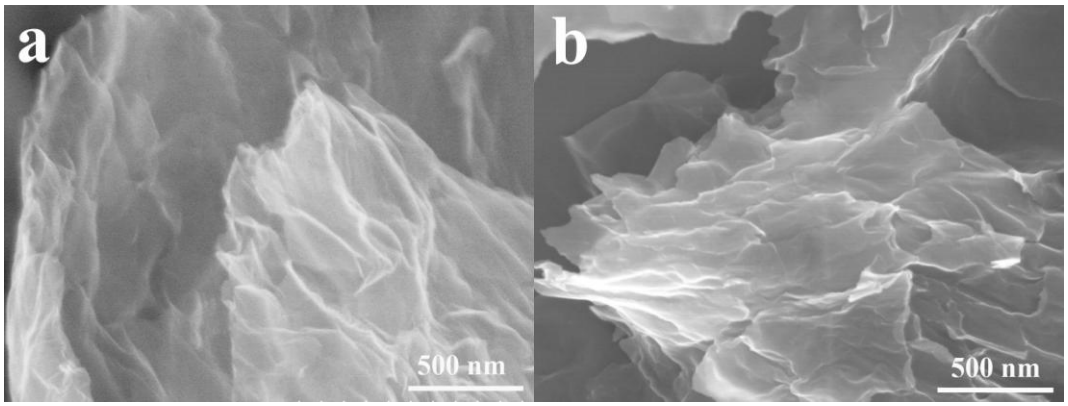

Figure S2. SEM images of the as-prepared (a) reduced graphene oxide and (b) GOPAA.

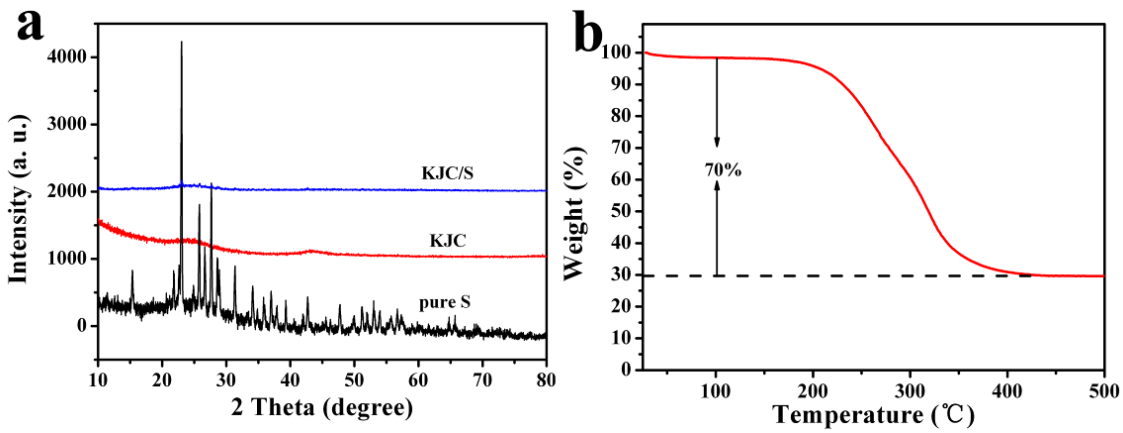

Figure S3. (a) XRD patterns of S, KJC and KJC/S composite. (b) TG curve of the KJC/S composite.

Two broad diffraction peaks located at ~25° and 43° for KJC and KJC/S (**Figure S3a**) correspond to the (002) and (101) diffractions of graphitic carbon, respectively [1]. There are no characteristic peaks of the crystalline sulfur in the KJC/S composite, demonstrating that sulfur is embedded in the KJC host. The sulfur content of the KJC/S composite is 70wt% based on the TG test (**Figure S3b**).

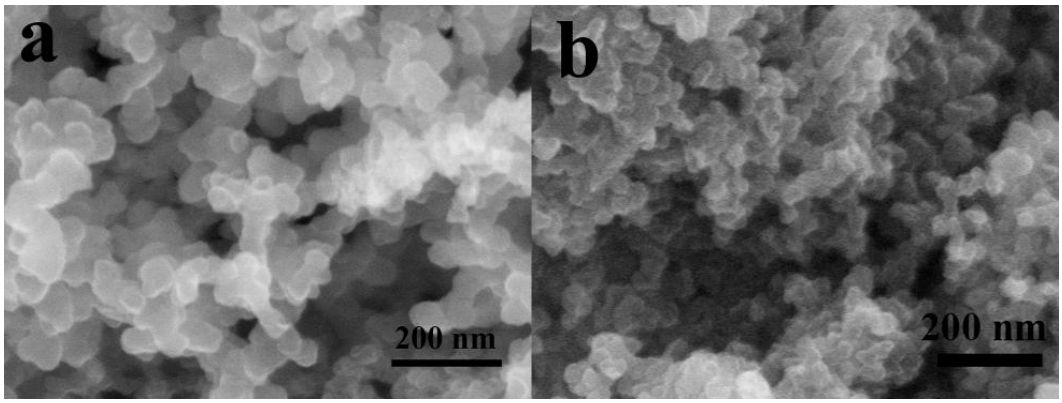

Figure S4. SEM images of (a) KJC and (b) KJC/S composite.

The KJC/S composite shows uniform morphology of small particles (**Figure S4b**). There is no apparent aggregation, indicating that sulfur completely diffuses into the pores of the KJC matrix by a capillary force during the heating process, which agrees well with the XRD analysis.

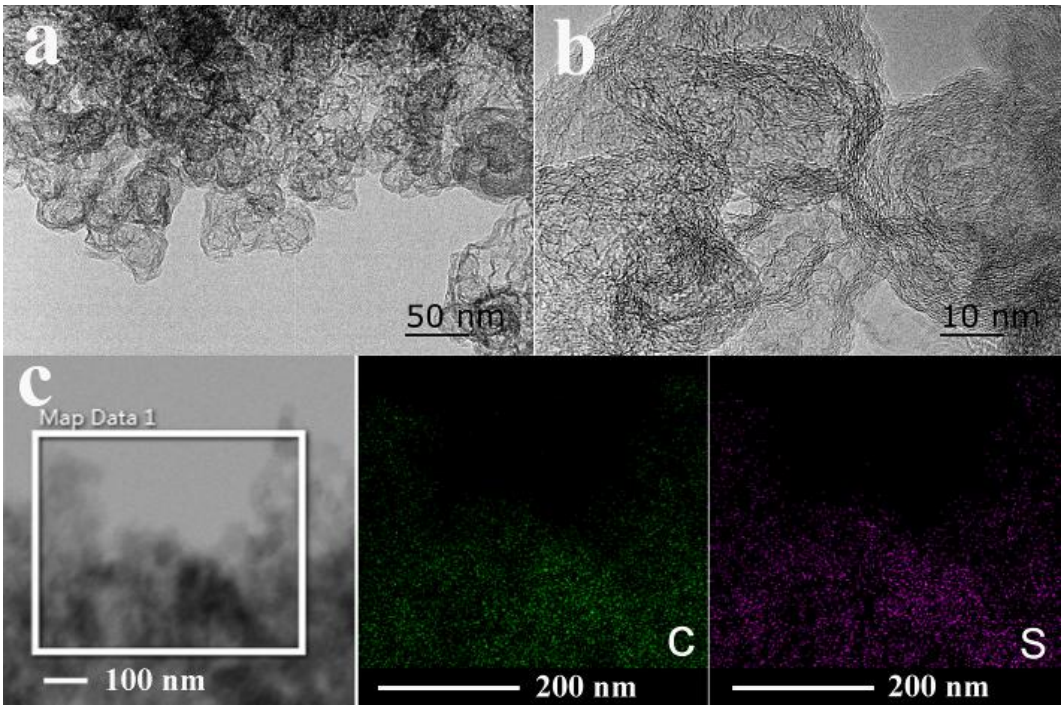

Figure S5. (a, b) TEM and (c) STEM images with corresponding elemental mapping of the KJC/S composite.

The nano-particles of KJC/S form a porous structure (**Figure S5b**), which can ensure enough volume to accommodate the volume expansion during cycling. Moreover, carbon and sulfur show homogeneous distribution in the KJC/S composite (**Figure S5c**).

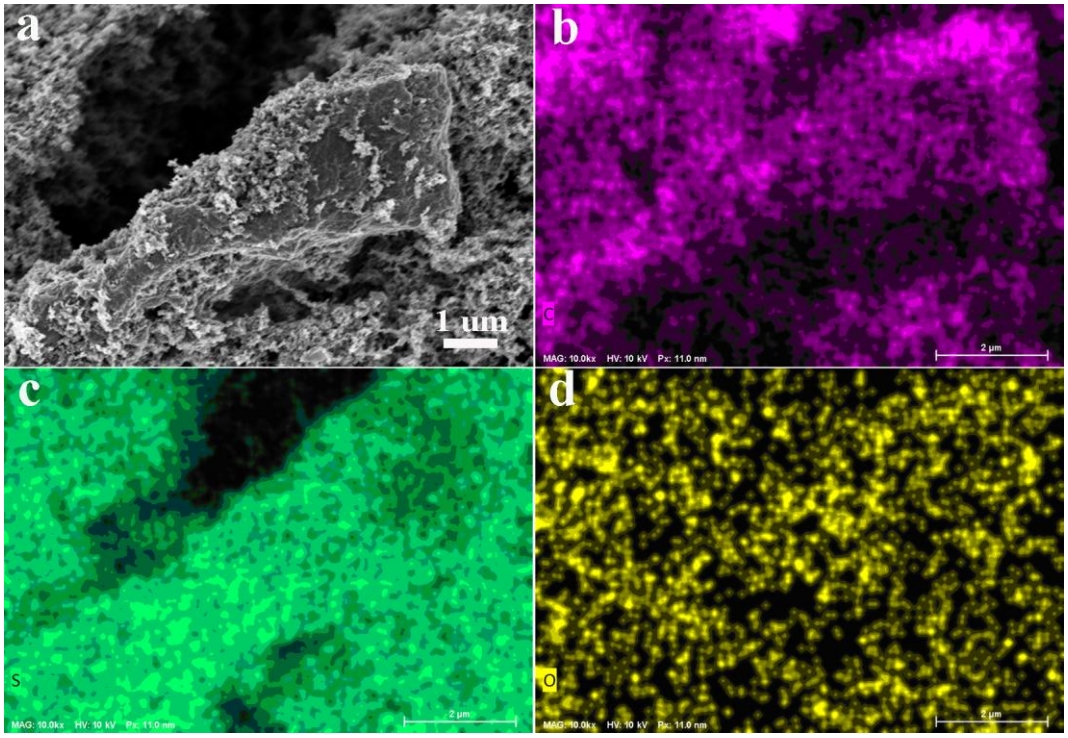

Figure S6. (a) SEM image of the KJC/S GOPAA electrode before cycling. Energy dispersive X-ray spectroscopy (EDS) elemental maps of (b) carbon, (c) sulfur, and (d) oxygen for the region shown in (a).

Energy dispersive X-ray spectroscopy (EDS) elemental maps confirm the uniform distribution of carbon, sulfur, and oxygen in the KJC/S GOPAA electrode before cycling.

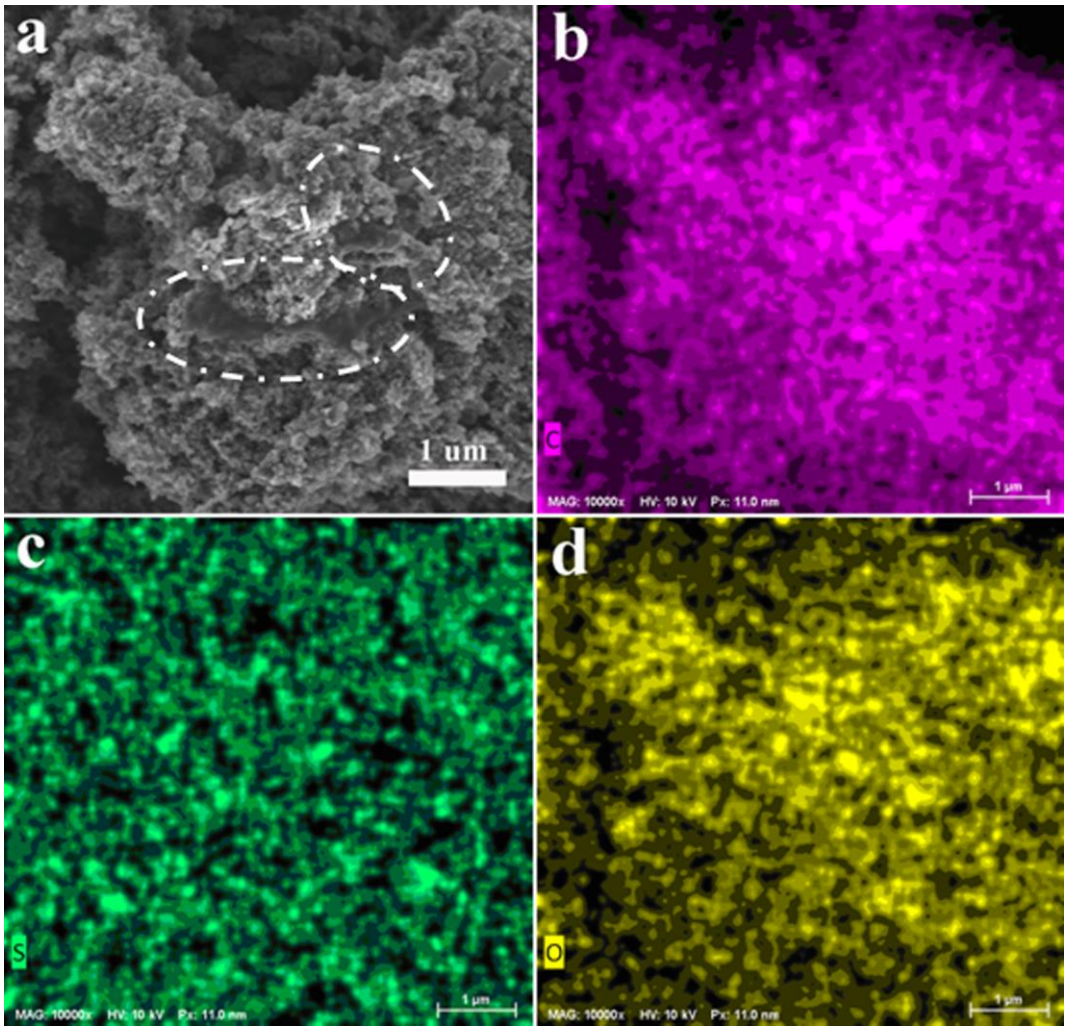

Figure S7. (a) SEM image of the cycled KJC/S GOPAA electrode. EDS elemental maps of (b) carbon, (c) sulfur, and (d) oxygen for the region shown in (a).

The KJC/S GOPAA electrode after 100 cycles at 0.5 C was washed with 1, 3-dioxolane and 1, 2-dimethoxyethane in the glovebox and then was characterized by SEM. A layer of nonconductive material is shown on the reduced graphene oxide (the circle in **Figure S7a**), which suggests that the reduced graphene oxide could provide active sites for the reversible deposition of Li_2S/Li_2S_2. EDS elemental maps (**Figure S7b-d**) indicate the uniform distribution of carbon, sulfur, and oxygen in the cathode.

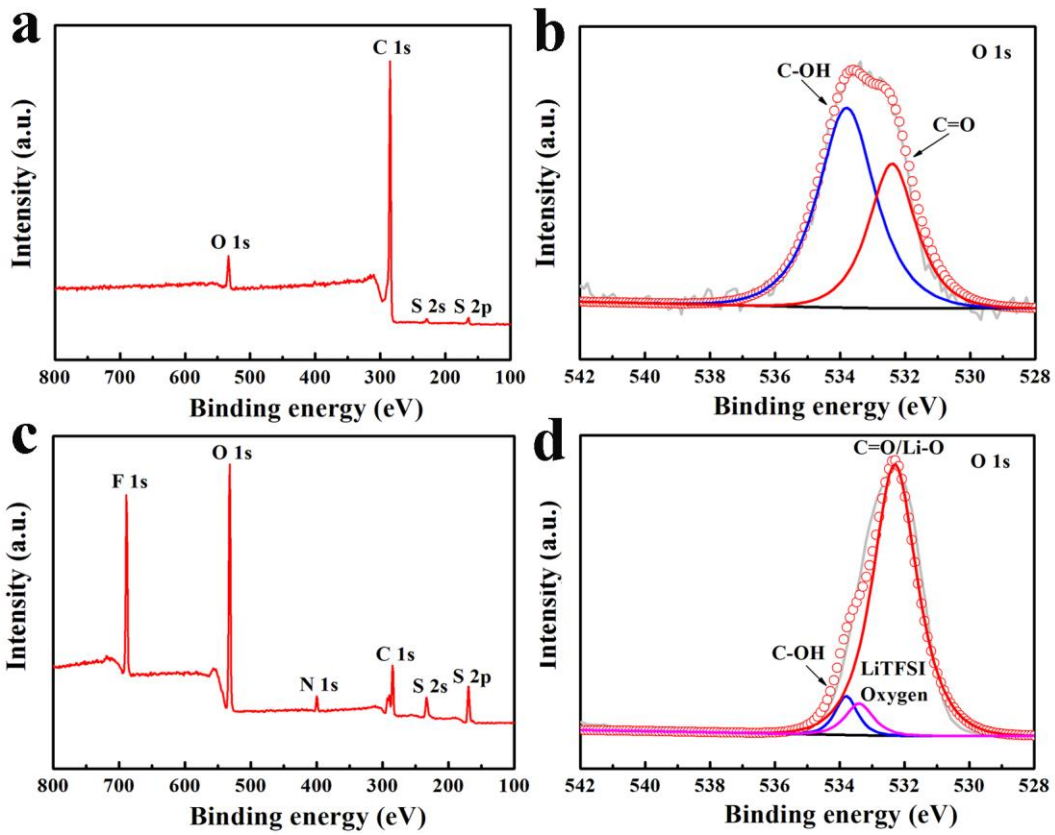

Figure S8. X-ray photoelectron spectroscopy (XPS) spectra of (a) the KJC/S GOPAA electrode before cycling and (c) the cycled KJC/S GOPAA electrode. O 1s XPS spectra of (b) the KJC/S GOPAA electrode before cycling and (d) the cycled KJC/S GOPAA electrode.

The KJC/S GOPAA electrode is composed of oxygen, carbon, and sulfur by the XPS analysis (**Figure S8a**). In the O 1s spectra of the KJC/S GOPAA electrode before cycling, the peaks at 533.8 and 532.4 eV correspond to the C-OH and C=O bonds from GOPAA [2] (**Figure S8b**). The cycled KJC/S GOPAA electrode is composed of fluorine, oxygen, nitrogen, carbon, and sulfur (**Figure S8c**). The fluorine and nitrogen elements are from LiTFSI. In the O 1s spectra of the cycled KJC/S GOPAA electrode, the peak at 533.4 eV is attributed to the LiTFSI oxygen [3] and the peak at 532.4 eV corresponds to the Li–O bond overlaid with the C=O bond [4] (**Figure**

S8d). The Li-O bond appearance demonstrates that PAA could chemically adsorb lithium polysulfides, thereby improving the electrochemical performance of Li-S batteries.

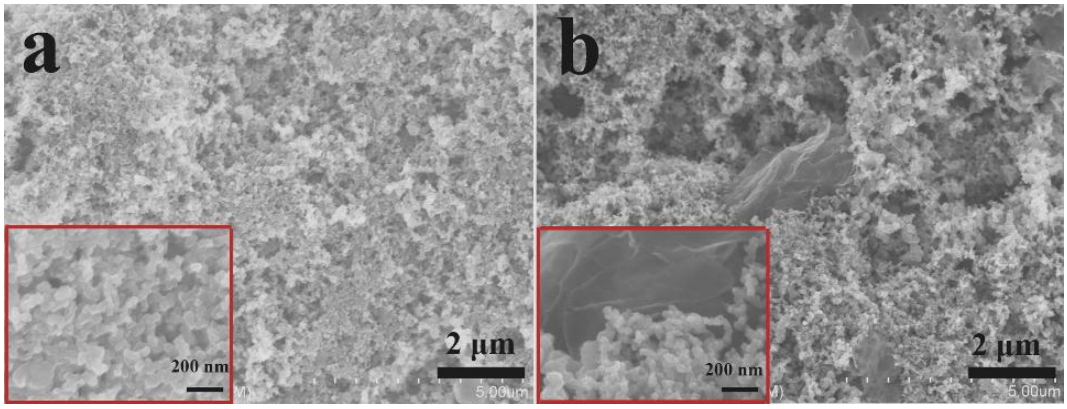

Figure S9. SEM images of pure sulfur electrodes with (a) PAA binder, and (b) PAA binder and RGO conductive additive.

In order to further verify the excellent performance of Li-S batteries with the GOPAA binder, pure sulfur is selected as active material. The ratio of sulfur, conductive agent, and binder was 60:25:15. There are three kinds of binder system: PAA, GOPAA, and 90wt% PAA with 10wt% RGO by the physical mixing. The distribution of each composition in sulfur cathodes is observed *via* SEM. The electrode with PAA binder shows a porous morphology and is consisted of small nanoparticles in **Figure S9a**. It is inferred that the small particles are acetylene black and sulfur powders are absorbed on the surface of acetylene black. PAA is hard to be observed from the SEM image. For the electrode with PAA as binder and RGO as conductive additive, RGO is occured in the electrode (**Figure S9b**).

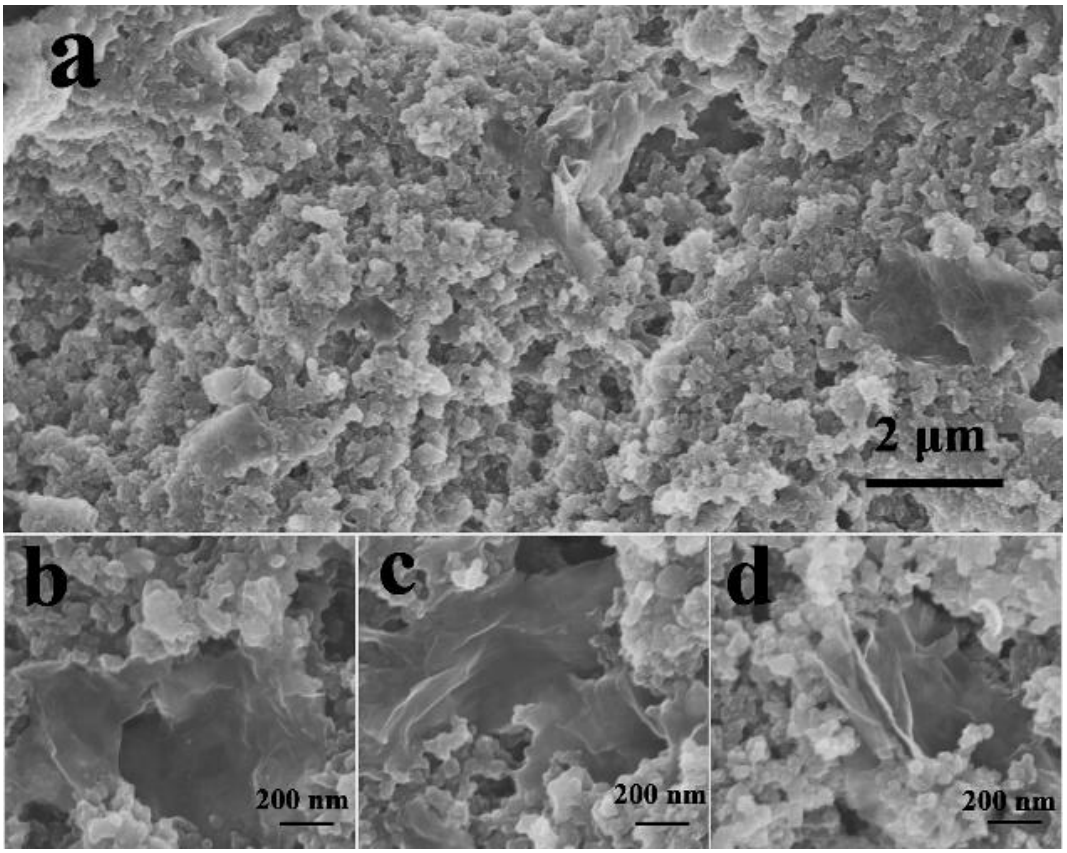

Figure S10. SEM images of pure sulfur electrode with GOPAA binder.

When GOPAA is applied in sulfur electrode, RGO nanosheets run through the electrode with a uniform distribution (**Figure S10a**). It can be seen clearly that some particles are covered and wrapped with RGO sheets (**Figure S10b, c, d)**. RGO penetrated in the cathode can improve the electronic conductivity of the electrode, especially favour the active materials far from the current collector and is conducive to fast electron transport.

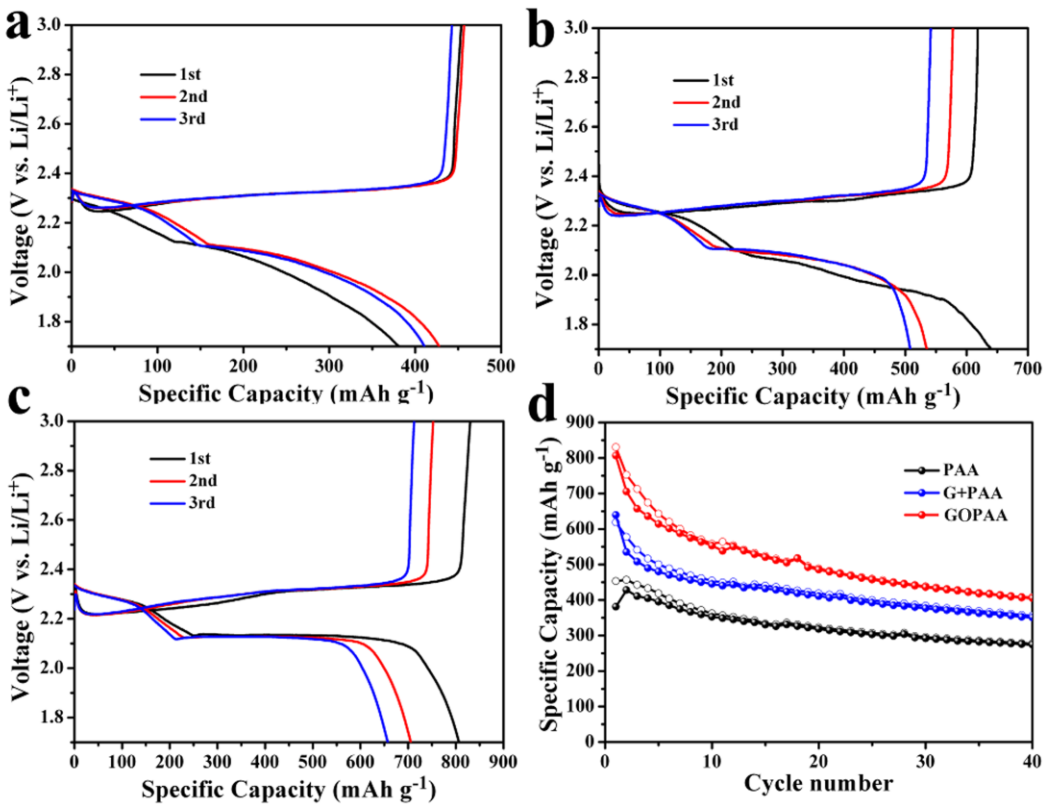

Figure S11. The charge-discharge voltage profiles of initial three cycles of different electrodes with (a) PAA as binder, (b) PAA binder and RGO conductive additive, and (c) GOPAA as binder at 0.1C. (d) Cycle performances of the three different electrodes at 0.1C.

The charge-discharge profiles of these three electrodes at 0.1 C are shown in **Figure S11**. When PAA is used as binder, the profiles show a severe polarization and there is no obvious plateau (**Figure S11a**). And the initial specific capacity of the PAA electrode is only 450 mAh g^{-1}, indicating the poor conductivity of the whole electrode. The electrode with the PAA binder and RGO conductive additive shows two unconspicuous plateaus, indicating two reduction reactions of sulfur active materials. The Li-S battery has an initial capacity of 640 mAh g^{-1} (**Figure S11b**). As shown in **Figure S11c**, the discharge curves of the pure sulfur electrode with GOPAA exhibit a typical two-plateau behavior of a sulfur cathode, corresponding to the formation of the long-chain and short-chain lithium polysulfide at ~2.3 V and 2.1 V, respectively. The electrode with

GOPAA shows the highest initial specific capacity of 850 mAh g^{-1} and a high remained specific capacity (**Figure S11d**). The simply physical-mixed PAA and RGO do not contribute to the enhancement as significantly as the composite binder.